Bioorganic & Medicinal Chemistry xxx (xxxx) xxxx

Contents lists available at ScienceDirect

Bioorganic & Medicinal Chemistry

journal homepage: www.elsevier.com/locate/bmc

Design and optimization of a series of 4-(3-azabicyclo[3.1.0]hexan-3-yl) pyrimidin-2-amines: Dual inhibitors of TYK2 and JAK1

Andrew Fensome[a,*], Catherine M. Ambler[b], Eric Arnold[b], Mary Ellen Banker[b], James D. Clark[c], Martin E. Dowty[a], Ivan V. Efremov[a], Andrew Flick[b], Brian S. Gerstenberger[a], Roger S. Gifford[c], Ariamala Gopalsamy[a], Martin Hegen[c], Jason Jussif[c], David C. Limburg[b], Tsung H. Lin[c], Betsy S. Pierce[b], Raman Sharma[b], John I. Trujillo[b], Felix F. Vajdos[b], Fabien Vincent[b], Zhao-Kui Wan[a], Li Xing[a], Xiaojing Yang[a], Xin Yang[b]

[a] Medicine Design, Pfizer Inc, 1 Portland Street, Cambridge, MA 02139, United States
[b] Medicine Design, Pfizer Inc, Eastern Point Road, Groton, CT 06340, United States
[c] Inflammation and Immunology, Pfizer Inc, 1 Portland Street, Cambridge, MA 02139, United States

ARTICLE INFO

Keywords:
TYK2
JAK1
Kinase
Autoimmune
Inflammation
Psoriasis
Arthritis

ABSTRACT

Herein, we disclose a new series of TYK2/ JAK1 inhibitors based upon a 3.1.0 azabicyclic substituted pyrimidine scaffold. We illustrate the use of structure-based drug design for the initial design and subsequent optimization of this series of compounds. One advanced example **19** met program objectives for potency, selectivity and ADME, and demonstrated oral activity in the adjuvant-induced arthritis rat model.

1. Introduction

The Janus kinases (JAK) are signaling molecules in the JAK/STAT (signal transducer and activator of transcription) pathways, which play a key role in intracellular signaling to extracellular cytokine signals.[1] Inhibition of the JAK kinases (TYK2, JAK1, JAK2 and JAK3) has received considerable interest for therapeutic intervention in auto-immune disease, and this area has been reviewed recently.[2] Whilst multiple compounds are in clinical development, only four compounds have been approved by the US FDA, Fig. 1. Xeljanz™ (tofacitinib) **1**, a potent inhibitor of JAK1 which also inhibits JAK2, JAK3 and with weaker inhibition of TYK2, was approved for rheumatoid arthritis, ulcerative colitis and psoriatic arthritis. The JAK1/JAK2 inhibitor Olumiant™ (baricitinib) **2** is approved for rheumatoid arthritis and Jakafi™ (ruxolitinib) **3** (JAK1/JAK2 inhibitor) has approvals for myelofibrosis, polycythemia vera and acute graft versus host disease.[3–5] The JAK1 selective inhibitor Rinvoq™ (upadacitinib) **4** was approved in 2019 for the treatment of rheumatoid arthritis.[6] We have previously reported upon PF-06700841 **5,** a TYK2/JAK1 inhibitor currently in Phase 2 clinical studies for psoriasis, hidradenitis suppurativa, vitiligo, atopic dermatitis, alopecia areata, psoriatic arthritis, lupus, ulcerative colitis and Crohn's disease.[7,8] Bristol Myers-Squibb are studying a TYK2 inhibitor, BMS-986165 **6**, that binds to the pseudokinase JH2 domain of TYK2 in multiple indications.[9,10]

In the current work, we were interested in developing a dual inhibitor of both JAK1 and TYK2. The JAK1 activity would inhibit the γ-common chain cytokines (*e.g.* interleukin (IL-)2, IL-4, IL-7, IL-9, IL-15, IL-21), IL-6 and Type I and II interferons, precedented by the clinically approved agents. The γ -common chain cytokines play an important role in both innate and adaptive immune systems, and have important function in the development of key inflammatory cell types (T, B, NK and innate lymphoid cells), important in many autoimmune conditions.[11]

The TYK2 component would introduce to the profile inhibition of IL-23 and IL-12 signaling, supported by clinical data from monoclonal antibodies to IL-12 and IL-23 and associated pathway proteins.[12] In genome-wide association studies, TYK2 loss of function polymorphisms are shown to provide protection from multiple auto-immune diseases, including psoriasis, rheumatoid arthritis, systemic lupus erythematosus and inflammatory bowel disease.[13] Inhibition of both JAK1 and TYK2 is

* Corresponding author.
E-mail address: Andrew.Fensome@Pfizer.Com (A. Fensome).

https://doi.org/10.1016/j.bmc.2020.115481
Received 5 February 2020; Received in revised form 25 March 2020; Accepted 27 March 2020
0968-0896/ © 2020 Elsevier Ltd. All rights reserved.

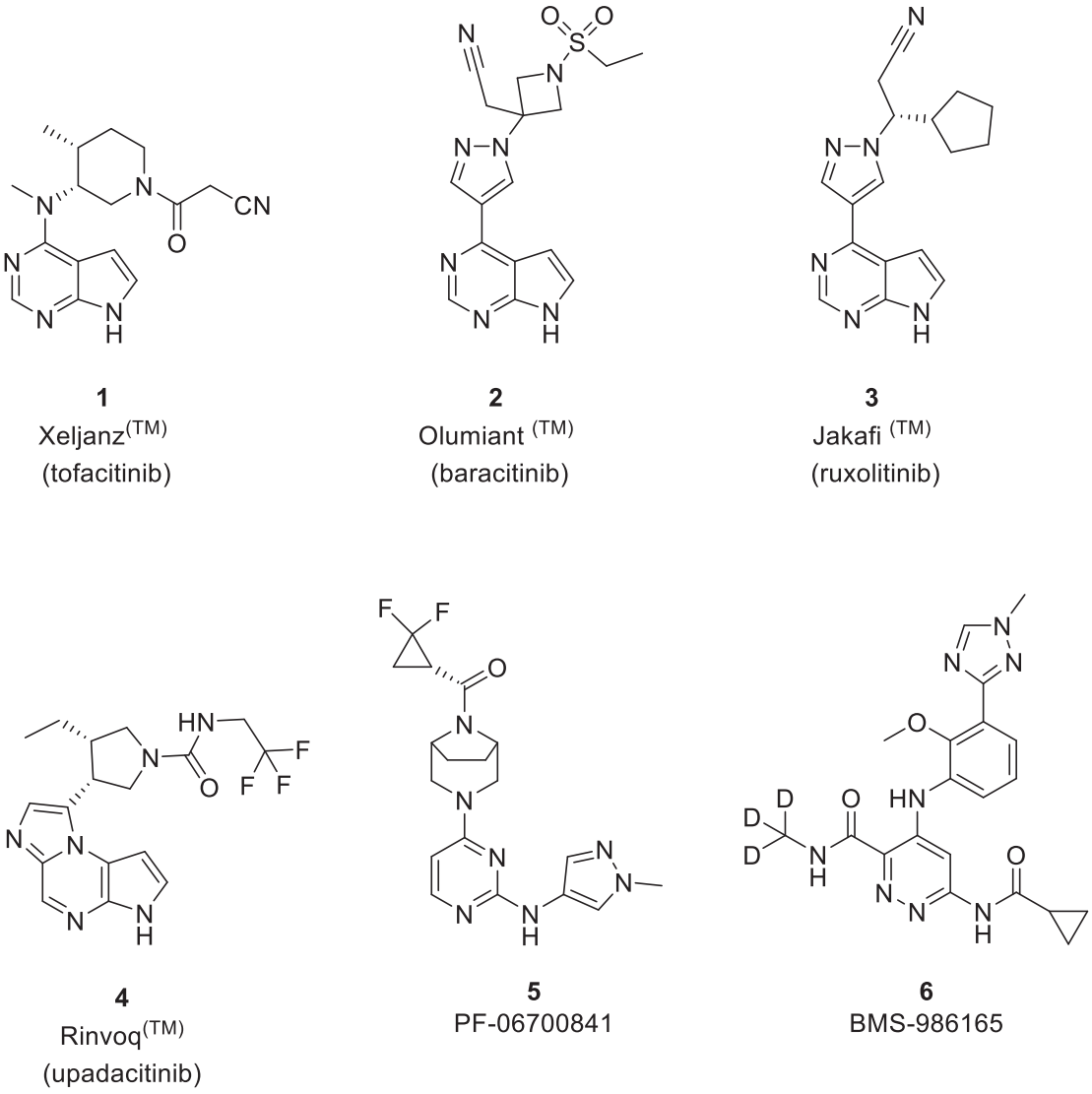

Fig. 1. Reference JAK inhibitors **1–6.**

hypothesized to be useful in multiple autoimmune diseases including, including psoriasis, psoriatic arthritis, lupus erythematosus and inflammatory bowel disease, by inhibiting type I interferon signaling (JAK1/TYK2), together with JAK1 driven γ -common chain cytokine and IL6 inhibition in combination with IL12 and IL23 inhibition in one molecule.

In an earlier manuscript we disclosed the discovery and initial characterization of PF-06700841 **5**.[7] In that paper we discuss our program objectives, derived from clinical and preclinical PK:PD relationships for tofacitinib (Xeljanz ™) **1**, and the utility of human whole blood assays to study cytokine inhibition in a standardized set of primary cell assays. With this understanding we projected that efficacy across autoimmune diseases would be driven by average (C_{av}) IC_{80} coverage of interferon alpha (IFNα), the primary target of TYK2 and JAK1 inhibition. To reduce JAK2 mediated effects on red blood cell differentiation, EPO inhibition ($CD34^+$ cells spiked into human whole blood) would be limited to $C_{av} \leq IC_{30}$. For candidate level molecules a predicted human PK model would be established to calculate projected cytokine inhibition levels, relative to IFNα IC_{80}. for the expedience of daily SAR and to allow us to understand selectivity against EPO signaling, a calculated C_{av} inhibition or IC_{XX}* was used based upon the IFNα IC_{80} and EPO IC_{50} from whole blood assays (IC_{XX}* = 100*((IC_{80} IFNα)/(IC_{80} IFNα + IC_{50} EPO)). Our objective was to drive potency on IFNα IC_{80}, whilst maximizing the window for EPO inhibition, with a target EPO IC_{xx}* ≤ IC_{30}. As a reference For PF-06700841 **5**, the EPO IC_{xx} = IC_{17}.[7]

As part of the earlier work we reported on molecules such as the [3.2.1] ring systems **7** and **8**, Fig. 2, Table 1.[7] We also investigated smaller bridged systems such as **9** (IC_{50} = 209 and 3900 nM, for TYK2 and JAK1 respectively). This latter compound was less potent than the [3.2.1] series molecules and lacked the balanced TYK2/JAK1 potency profile we were seeking.

To increase potency, we were interested in a strategy where we could form a hydrogen bond interaction with the catalytic aspartate, Asp-1041. We built a model of **9** docked into the TYK2 catalytic domain, from which the proximity (3.4 Å) between the bridge head carbon and the carboxylate of Asp-1041 can be seen. We hypothesized that the endocyclic amide nitrogen of the [3.1.1]diaza-bicyclic ring system (**i**) could be moved into an exocyclic position, to interact with ASP-1041. In earlier work we had found that a bridged ring system was optimal for potency, due to reduced degrees of freedom, and the ability to project into the lower lipophilic portion of the binding site.[7] To this end we built a new C—C bond to form a [3.1.0] ring system (**ii**), compounds **10–12** (Table 2) the amide N—*H* of which would be available to form the desired H-bond, Fig. 3.

Functional enzymatic activity against the four JAK kinases was

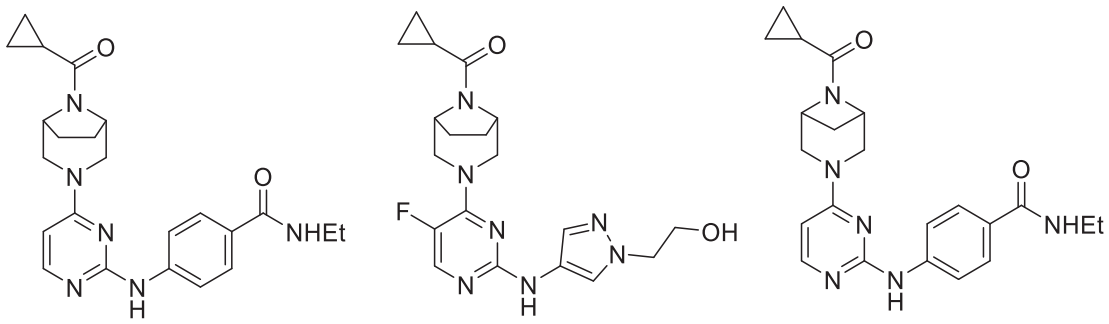

Fig. 2. Structures of compounds **7**–**9**.

Table 1
Enzymatic potencies and efficiency data for compounds **7** – **9**.

	IC_{50} (nM)[a]					
Compound	**TYK2**	**JAK1**	**JAK2**	**JAK3**	**LogD[b]**	**TYK2 LipE[c]**
7	32	122	329	> 10,000	1.8	5.9
8	55	81	260	2531	1.8	5.8
9	209	3900	9644	> 10,000	1.7	5.2

[a] Compounds were assayed at least twice, and the IC_{50} reported as the geometric mean.
[b] Shake flask logD at pH 7.4.
[c] LipE = pIC_{50} – LogD.

obtained using a PerkinElmer LabChip® EZ Reader assay, under pseudo-physiological conditions, with ATP at a concentration of 1 mM, as reported previously.[14] Under these conditions we are able to compare JAK enzyme potencies directly without taking into account the K_M for ATP for each target. Moreover, as previously reported, the pseudo physiological conditions more closely correlate with cellular functional readouts with minimum potency shifts.[14] Cellular data was obtained from human whole blood assays where we studied inhibition of STAT phosphorylation *via* flow cytometry, experimental conditions were reported previously.[7] Each signaling pathway was activated with a near maximal concentration of the desired cytokine. EPO signaling was determined in human whole blood spiked with $CD34^+$ cells.[7] Whole blood data was corrected for protein binding to provide an estimate of unbound potency (assuming blood: plasma ratio = 1), thereby allowing comparisons to be made between compounds, independent of plasma binding. Protein binding data was either measured or calculated using a QSAR model.

Following on from our earlier work we decided to make the [3.1.0] analog of **8** - and allow us to make matched pair comparisons, Fig. 4, Table 2. In earlier work we had shown in molecules similar to compound **8**, that the 5-fluoro pyrimidine derivative was slightly more potent than the 5-H pyrimidine congener, and as such in the current work elected to retain the 5-fluorine substituent.[7] As such we prepared **10** which proved to be the eutomer (IC_{50} = 139, 774, 5663 and > 10,000 nM respectively for TYK2, JAK1, JAK2 and JAK3). In human whole blood the compound was active but with modest potency against IFNα signaling. The distomer, compound **11**, proved to be much weaker (TYK2 IC_{50} = 5303 nM, JAK1 IC_{50} > 7359 nM).

Compound **10** was crystalized with the catalytic JH1 domains of both TYK2 and JAK1, Fig. 5**a and b** respectively. Gratifyingly, the structure confirmed our design hypothesis, with a hydrogen bond being formed between the amide N–*H* and the catalytic Asp-1041 in TYK2 and Asp-1021 in JAK1, with the *S*-stereochemical configuration at this center. This stereochemical feature was consistent throughout the series. The structures also show the two differential residues between the two ATP binding sites: Ile-960 in TYK2 which is Val-938 in JAK1. Val-981 in Tyk2 makes the typical hinge donor/acceptor hydrogen bonds with the ligand, whereas in Jak1 this residue is Leu-959. A solvent front hydrogen bond is also made between the ethanol side chain of the molecule and the backbone N–*H* of either Ser-985 (TYK2) or Ser-963 (JAK1). A lipophilic pocket below the cyclopropane of the [3.1.0] ring system is also evident in the structure. The ADME characterization of the compound encouraged us to explore this chemotype further: the compound had reasonable kinetic aqueous solubility (278 μM at pH 7.4), moderate passive permeability[15] (MDCK-II mean P_{APP} = 4.4 × 10^{-6} cm/*sec*) and good stability in human liver microsomes (< 8 μL/min/mg), consistent with a LogD = 1.75.

In efforts to increase potency, we first turned our attention to the lipophilic pocket at the bottom of the binding site. The addition of an endo methyl group to the cyclopropane **12**, gave a small boost in potency (IC_{50} = 57 and 157 nM for TYK2 and JAK1 respectively), but with no net gain in lipophilic efficiency (LipE = 5.41 and 5.45 for **10** and **12** respectively). The increase in potency translated into the human whole blood assay (IFNα $IC_{50(u)}$ = 443 (1 1 1) nM) with good

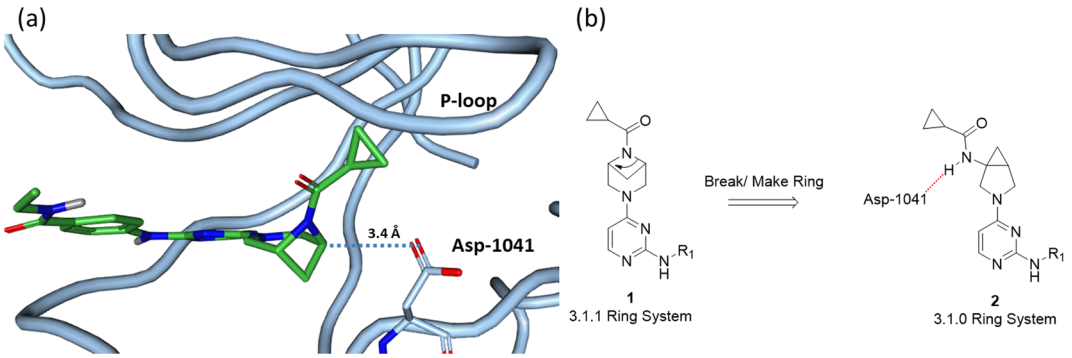

Fig. 3. Initial design strategy for [3.1.0] ring system: (a) docked binding mode of compound **9** in TYK2 ATP binding site; (b) break-a-ring/ make-a-ring design of [3.1.0] ring system.

ARTICLE IN PRESS

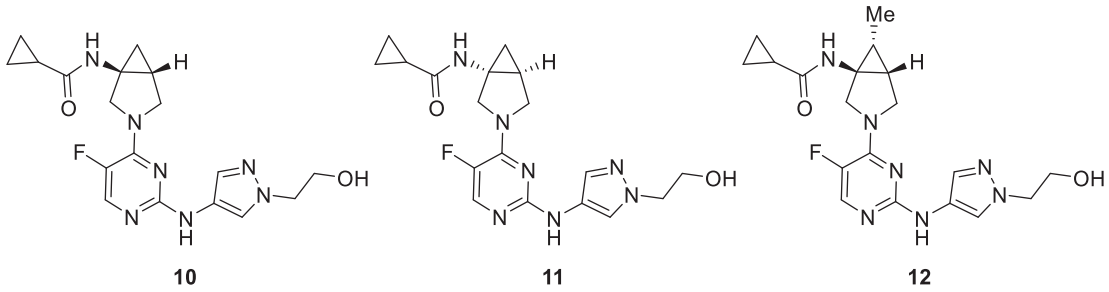

Fig. 4. Structures of compounds **10–12**.

Table 2
JAK Enzymatic potencies, human whole blood data and efficiencies for compounds **10 – 12**.

Compd.	IC_{50} (nM)							HWB IC_{50} (nM)			HWB IFNα IC_{80} (nM)[a]	EPO IC_{XX}*
	TYK2[a]	JAK1[a]	JAK2[a]	JAK3[a]	LogD[b]	Fu[c] (%)	Tyk2 LipE[d]	IFNα[a]	$IFN\alpha_{(u)}$[e]	EPO[a]		
10	139	774	5663	> 10000	1.74	0.41	5.4	1523	621	> 20000	6092	< 23
11	5303	> 7359	> 10000	> 10000	1.75		3.8	ND	ND	ND	ND	ND
12	57	157	1617	> 8458	2.10	0.31	5.4	443	111	15,264	1772	10

[a] Compounds were assayed at least twice, and the IC_{50} reported as the geometric mean.
[b] Shake flask logD at pH 7.4.
[c] Human plasma free fraction measured at 2 μM compound concentration.
[d] LipE = pIC_{50} – LogD.
[e] Free IC_{50} = IFNα HWB IC_{50}* human plasma free fraction.

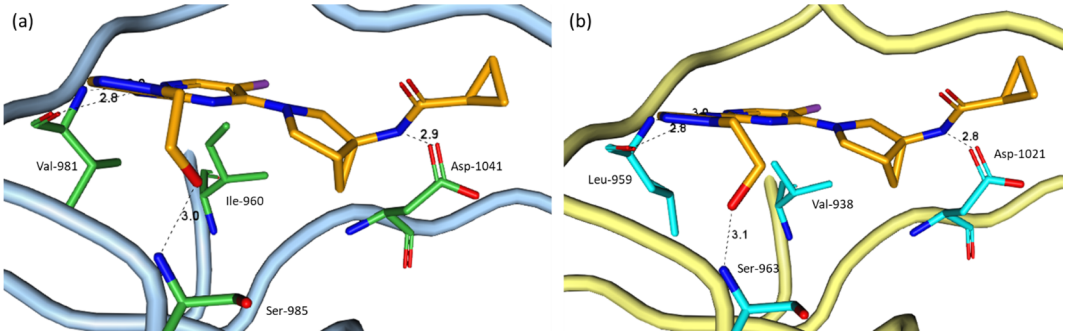

Fig. 5. Compound **10** crystallized with TYK2 (a) and JAK1 (b) showing H-bond to Asp-1041 and Asp-1021 respectively. The structures also illustrate the differential residues between TYK2 and JAK1: Val-981 to Leu-959 and Ile-960 to Val-938, respectively.

selectivity over EPO signaling (EPO HWB IC_{50} = 15,264 nM, IC_{XX}* = IC_{10}).

To better guide efforts to increase potency further, we turned to computational analysis. Starting with the crystal structure of **10** bound to TYK2, we simulated water energetics for the apo protein, Fig. 6, Table 3.[16] From the simulation, three water molecules were shown to be proximal to the cyclopropane. Simulated apo waters W1 and W2 would be displaced upon ligand binding. W1 is a moderately unstable water, whilst W2 was the highest energy water in the simulation, displacement of which could theoretically improve potency. The third water, W3, was also predicted to be unstable (ΔG = 3.04, ΔH = 1.23 and –TΔS = 1.8), displacement of this water presented an additional opportunity to increase potency.

We first prepared the diastereomeric *trans*-cyano cyclopropyl amides **13** and **14**, Fig. 7, Table 3. Crystallography showed that both isomers would be able to displace the high energy simulated water W3 as well as W2, Fig. 8. Gratifyingly, both compounds were more efficient, potent inhibitors of TYK2 and JAK1 than the parent **10** (Compound **13** IC_{50} = 29 and 18 nM for TYK2 and JAK1, TYK2 LipE = 6.44; Compound **14** IC_{50} = 67 and 304 nM for TYK2 and JAK1, TYK2 LipE = 6.04, respectively). The more potent of the two compounds with *R,R*-cyclopropyl stereochemistry, compound **13**, was overall less selective for JAK2 and JAK3 (**13** IC_{50} = 340 and 949 nM for JAK2 and JAK3; **14** IC_{50} = 2167 and > 10,000 nM for JAK2 and JAK3). The increase in enzymatic potency for this modification translated into cells for the more potent nitrile isomer. In the human whole blood IFNα assay, **13** was more active than the parent **10** (IFNα $IC_{50(u)}$ = 153 (73) nM). Unbound potency values are needed when comparing compounds whereby plasma protein binding is accounted for. This improved unbound whole blood potency is a consequence of improved potency for both TYK2 and JAK1, bearing in mind that IFNα utilizes both TYK2 and JAK1 for signal transduction. For the less active isomer **14**, the same whole blood potency gains were not realized compared with analog **10**.

We next combined the cyano-cyclopropane and the endo methyl group to provide compounds **15** and **16**. The expected additive increase in TYK2 potency was not achieved, although the JAK1 potency did improve. Compound **15**, with *R,R*-stereochemistry, was more active on TYK2 and JAK1 but again lacked the desired family selectivity. The *S,S*-cyano-cyclopropane **16** was more interesting, showing balanced activity against the primary enzymatic targets (TYK2 and JAK1 IC_{50} = 32 and 41 nM, respectively). However, in the IFNα human whole blood assay the compound was relatively weak ($IC_{50(u)}$ = 971 (3 7 4) nM). We

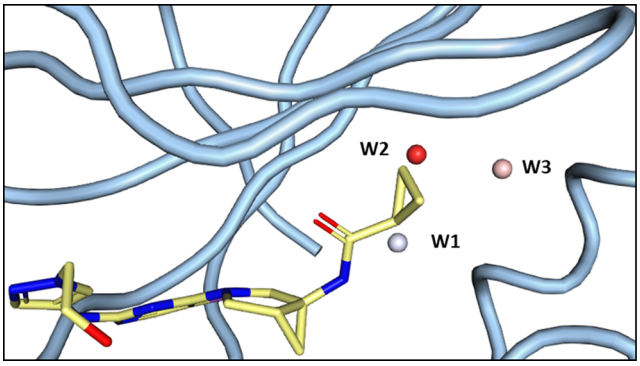

Water	ΔG	ΔH	-TΔS
1	2.44	-0.59	3
2	6.83	4.38	2.45
3	3.04	1.23	1.8

Fig. 6. Compound **10** overlaid onto simulated apo water molecules in the TYK2 ATP binding site. Table 3. Energetics for simulated apo waters W1 – W3.

hypothesized that the cellular potency was hampered by a lack of permeability (MDCKII mean P_{app} = 1.2 × 10^{-6} cm/*sec*).

Whilst the *N*-hydroxyethyl substituent on the pyrazole did not pose a secondary metabolism liability (human hepatocyte Clint < 6 μL/min/million cells for **10** and **12**) for this series of compounds, it did present additional polarity, and an H-bond donor/acceptor which could influence permeability. To this end we made the simple *N*-methyl pyrazole of the above compounds to address this issue. As would have been expected from the previous data, the R,R-cyclopropane **17** was indeed the more active isomer on TYK2 and JAK1, however again showed potent activity on JAK2 and in particular JAK3 (IC_{50} = 32, 11, 228 and 225 nM for TYK2, JAK1, JAK2, JAK3 respectively). The less potent *S,S*-isomer **18** had similar enzymatic potency to the hydroxyethyl congener **16**. As would be expected, the LogD of these two

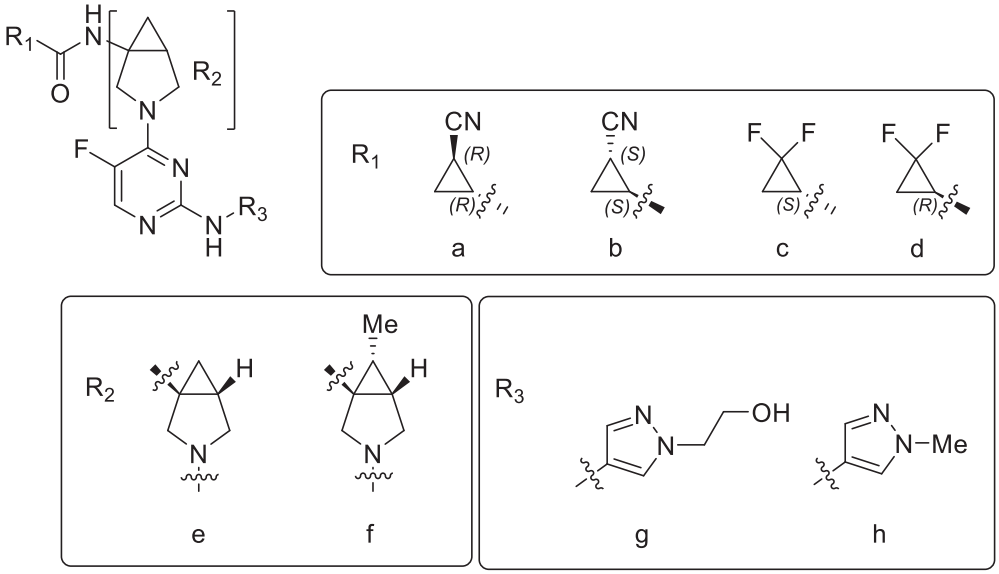

Fig. 7. Structures of compounds **13–20**.

Table 3
JAK Enzymatic potencies, human whole blood data and efficiencies for compounds **13 – 20**.

Compd.	R Group			IC_{50} (nM)							HWB IC_{50} (nM)			HWB IFNα IC_{80} (nM)[a]	EPO IC_{xx}*
	1	2	3	TYK2[a]	JAK1[a]	JAK2[a]	JAK3[a]	LogD[b]	Fu[c] (%)	Tyk2 LipE[e]	IFNα[a]	$IFNα_{(u)}$[f]	EPO[a]		
13	a	e	g	29	18	340	949	1.40	0.47[d]	6.4	153	73	13,017	612	4
14	b	e	g	67	304	2167	> 10000	1.43	0.42	6.0	1812	888	> 20000	7248	3
15	a	f	g	37	6	128	194	1.71		6.1	148	57	1492	592	28
16	b	f	g	32	41	676	2282	1.75	0.37[d]	6.0	971	374	12,850	3884	23
17	a	f	h	32	11	228	255	2.35	0.29	5.4	87	21	1942	348	15
18	b	f	h	49	81	1168	3225	2.32	0.35	5.3	421	104	9368	1684	15
19	c	f	h	29	41	652	4267	2.65	0.24	5.2	191	42	11,440	764	6
20	d	f	h	56	113	1132	4023	2.92	0.15	4.6	1733	414	18,837	6932	27

[a] Compounds were assayed at least twice, and the IC_{50} reported as the geometric mean.
[b] Shake flask logD at pH 7.4.
[c] Human plasma free fraction measured at 2 μM compound concentration.
[d] Calculated free fraction.
[e] LipE = pIC_{50} – LogD.
[f] Free IC_{50} = IFNα HWB IC_{50}* human plasma free fraction.

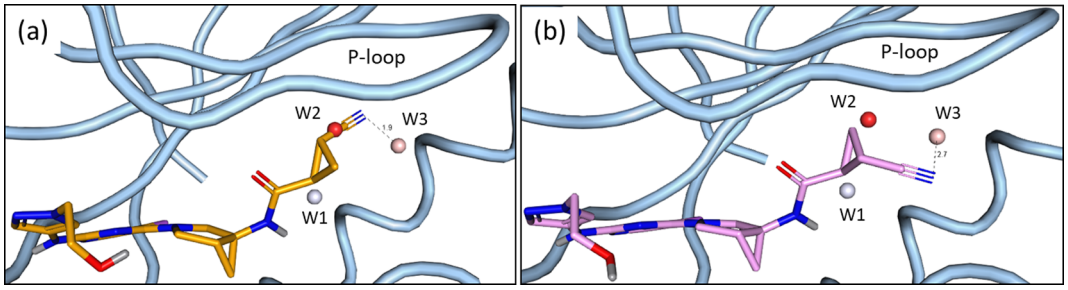

Fig. 8. Crystal structure of (a) Compound **13**/ TYK2 (2.09 Å) and (b) Compound **14**/ TYK2 (2.15 Å), overlaid with simulated apo waters W1, W2 and W3.

compounds was approximately 0.6 units higher, but most importantly the passive permeability improved noticeably (MDCKII mean P_{APP} = 12.9 and 13.8 × 10^{-6} cm/*sec* for **17** and **18**). This improved permeability brought with it an increase in cellular activity for the more selective compound **18** (IFNα HWB $IC_{50(u)}$ = 421 (104) nM), however this compound still did not meet the program goals for cellular potency. The EPO selectivity was in line with the JAK2 potency (EPO IC_{50} 9,368 nM, IC_{XX}* = IC_{15}).

In the cyno cyclopropyl amide series, the trend for the *R,R*-enantiomer being less selective (increased potency) than the *S,S*-isomer can be rationalized from the structure if we extrapolate across the JAK kinase family, Fig. 8. From the structure of compound **13** (*R,R*-enantiomer) with TYK2, we can see that the nitrile projects into the P-loop of the kinase, making interactions with the protein, Fig. 8**a**. In the case of the S,S-enantiomer, the nitrile functionality is projecting away from the P-loop, towards solvent, and hence has less interaction with the protein, Fig. 8**b**, which would engender greater selectivity.

Amongst the cyclopropane substitution patterns we tried in the program, the most fruitful was the difluorocyclopropane.[7] We prepared the difluoro cyclopropyl derivatives with the goal of increased cellular potency with a balanced JAK enzyme profile. Compound **19**, with *S*-stereochemistry at the cyclopropane chiral center, proved to have good potency against TYK2 and JAK1 (IC_{50} = 29 and 41 nM respectively, TYK2 LipE = 5.2), with promising selectivity against JAK2 and JAK3 (JAK2 and JAK3 IC_{50} = 652 and 4356 nM, respectively). In the IFNα human whole blood assay, the compound had good potency (IFNα HWB $IC_{50(u)}$ = 191 (42) nM; EPO HWB IC_{50} = 11,440 nM, IC_{XX}* = IC_6). In contrast, the isomeric cyclopropane **20** was a little less active on both TYK2 and JAK1 (IC_{50} = 56 and 113 nM respectively), which was inadequate to drive high cellular activity (IFNα HWB $IC_{50(u)}$ = 1733 (4 1 4) nM). The binding mode of compound **19** was consistent with compounds discussed thus far, Fig. 9. Of note in the structure is the projection of the two fluorine atoms up towards the P-loop of the protein. Consistent with our apo water hypothesis, water W2 would be displaced by the compound. The distal water W3 is also within proximity to the fluorine atom and may also be expected to be displaced.

Compound **19** was selected for further profiling against an expanded set of cytokines in human whole blood assays, the values are reported as unbound IC_{50}. Against the TYK2/JAK2 pathways IL-23 (pSTAT3) and IL-12 (pSTAT4) the compound had $IC_{50(u)}$ = 207 nM and 108 nM, respectively. Compound **19** inhibited the γ -common signaling pathways (JAK1/JAK3) represented by IL-21/pSTAT3 ($IC_{50(u)}$ = 319 nM), and IL-15/pSTAT5 ($IC_{50(u)}$ = 265 nM). Interferon-γ /pSTAT1 was inhibited by compound **19** with a whole blood $IC_{50(u)}$ = 265 nM. IL-10/pSTAT3 and IL-27/pSTAT3 signaling was inhibited by **19** with $IC_{50(u)}$ = 659 nM and 155 nM, respectively. Kinase selectivity was determined at both the K_M for ATP for each kinase, or at 1 mM in the Carna Bioscience panel, at a compound test concentration of 1 μM. Under the [ATP] at K_M conditions the compound had activity at 15 out of 307 kinases above 60% inhibition, and 20 targets between 30 and 60% inhibition, **Supplementary Table 1**. Under the 1 mM ATP conditions, compound **19** was active against 5 kinases at or above 16% inhibition: JAK3 (16.0%), TNK1 (50.6%), JAK2 (62.9%), JAK1 (87.0%) and TYK2 (90.2%). Against a promiscuity panel of 94 targets (internal and Cerep) compound **19** only showed activity for EGFR kinase ([ATP] = K_M, IC_{50} 4,110 nM, Cerep) and VEGFR2 ([ATP] = K_M, IC_{50} 284 nM, Cerep). Follow-up cellular assays for both EGFR and VEGFR2 were negative (Caliper Biosciences), supported by data from the Carna Biosciences panel for EGFR (1.3% inhibition at a test concentration of 1 μM ([ATP] = 1 mM)) and KDR/VEGFR2 (5.0% inhibition at a test concentration of 1 μM ([ATP] = 1 mM).

The *in vitro* metabolism was studied in human liver microsomes ($Cl_{int,u}$ < 8 μL/min/mg protein) and hepatocytes ($Cl_{int,u}$ 3.45 μL/min/million cells), which indicated low metabolic turnover. Plasma protein binding was moderate in rat (fraction unbound (f_u) 0.19) and human (f_u 0.24), with no significant blood to plasma partitioning (human Crbc/Cp

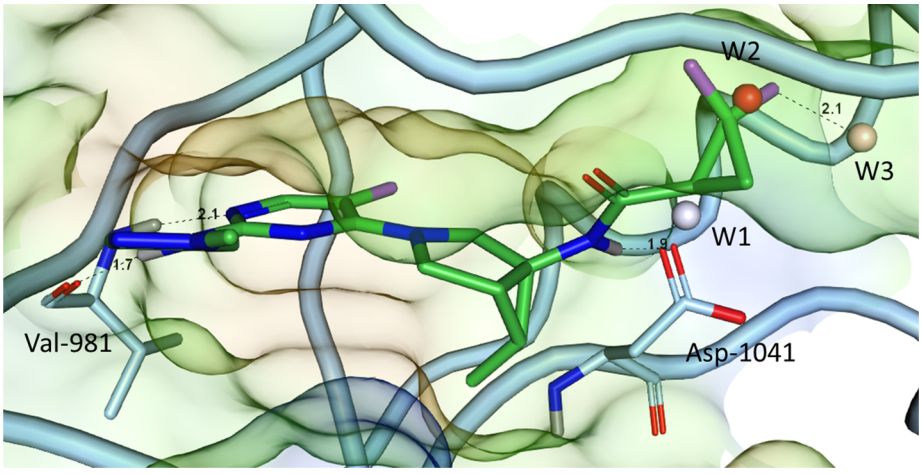

Fig. 9. Crystal structure of compound **19** bound to TYK2 ATP binding site (2.18 Å), overlaid with apo simulated waters W1 – W3.

1.15).

The physical properties of compound **19** were favorable for oral dosing with a molecular weight of 407.4, a measured LogD (pH 7.4) of 2.7, and a calculated TPSA of 88 Å^2. Compound **19** also showed high *in vitro* passive permeability (MDCKII mean P_{APP} = 17 × 10^{-6} cm/s). Aqueous solubility was 0.14 mg/mL at pH 6.5 and > 15 mg/mL at pH 2 from crystalline material. The pharmacokinetics of **19** were studied in Sprague − Dawley rats following intravenous and oral administration (1 and 3 mg/kg respectively), where the compound showed a plasma clearance of 13 mL/min/kg, a volume of distribution of 1.2 L/kg, and half life of 1.4 h. Following the 3 mg/kg oral dose, the observed C_{max} was 614 ng/mL, the AUC_{∞} was 2030 ng·h/mL with oral bioavailability of 54%.

Based on the physicochemical properties **19** was predicted by the Extended Clearance Classification System (ECCS) to be a class 2 compound with rate determining pathway of metabolic clearance.[17] Oxidative metabolites of **19** accounted for the primary routes of biotransformation in rat and *human in vitro* hepatic systems, consistent with CYP450 as the primary clearance route. Metabolic pathways included oxidation of the *N*-methyl pyrazole, *N*-demethylation (pyrazole), and *N*-dealkylation (loss of pyrazole). Metabolic clearance phenotyping of **19** indicated that CYP3A4 was likely the predominant mediator of metabolism. As the clearance mechanisms of **19** were determined to be mediated primarily by CYP450 metabolism (principally through CYP3A4), with limited renal and biliary clearance expected, human pharmacokinetic predictions were made using human liver microsomes and hepatocytes, as well as standard single species allometric scaling techniques, Table 4.

Cl_b: blood clearance; V_{ss}: volume of distribution at steady state; Fraction unbound plasma protein binding in rat and human were 0.19 and 0.24 respectively. Human clearance predictions from *in vitro* systems were scaled based on the well-stirred model or single species scaling from allometry.[18,19]

The overall average daily % cytokine inhibition profile (IC_{XX}) was calculated for **19** based upon the modelled C_{av} exposure of approximately 89 nM (unbound) at an expected efficacious dose of 75 mg QD, Fig. 10, Table 5.[20,21] Under these conditions JAK1/TYK2 driven IFNα inhibition is set at a target of IC_{80}. The IL-12 and IL-23 target cover (TYK2/JAK2) was IC_{61} and IC_{45}, respectively. IL-6 inhibition (JAK1/JAK2 or TYK2) *via* pSTAT1 in $CD34^+$ cells was IC_{48}. Contribution to the profile from the γ -common chain cytokines (JAK1/JAK3), represented by IL-15 and IL-21 were lower at IC_{39} and IL_{35}, respectively. IL-27 (JAK1/JAK2 or TYK2) and IL-10 (JAK1/TYK2) target cover was estimated to be at IC_{52} and IC_{20}, respectively. Importantly, the compound is expected to spare JAK2/JAK2-driven EPO signaling (IC_{06}) (see Fig 11.).

Compound **19** was studied *in vivo* in a rat adjuvant-induced arthritis (AIA) disease model.[22] Female Lewis rats immunized with complete Freund's adjuvant were orally dosed with **19** or vehicle for seven consecutive days after disease onset as measured by hind paw volume using plethysmography. Paw volumes and body weights were followed throughout the study. At the end of 7 days of dosing, plasma concentrations of **19** were assessed. Two studies were completed.

In the initial study, immunized rats were dosed QD with 3, 10, 30 or 100 mg/kg of **19** or vehicle (PO) (see supplemental information). Because a significant reduction in paw swelling was observed for all doses, a second study was conducted focused on lower doses (1, 5, 15 or 30 mg/kg **19** or vehicle control), Fig. 10. A significant reduction of hind paw swelling was observed with doses as low as to 3 mg/kg, **Supplemental Fig. 1**. Collective pharmacodynamics modeling of both studies using an E_{max} model fit indicated an unbound C_{av50} of approximately 199 nM (95% CI 134 – 294 nM), **Supplemental Fig. 2**.

In conclusion we designed a new series of [3.1.0] bicyclic TYK2/JAK1 inhibitors based upon a rational design starting from earlier work in our program. This new series was further optimized based on emerging SAR and relying upon crystal structures of key analogs and computational modelling and simulation. The lead analogs from this series, compound **19**, was demonstrated to have good *in vitro* and *in vivo* ADME properties. The predicted human PK and dose, and the projected JAK target cover successfully met the program objectives for a clinical candidate.

Table 4
Summary of predicted human blood pharmacokinetics of compound **19** from *in vivo* and *in vitro* systems

Method	Human Prediction	
	Cl_b (mL/min/kg)	V_{ss} (L/kg)
Human Liver Microsomes	1.4	
Human Hepatocytes	1.6	
Rat Single Species Scaling	3.5	1.5

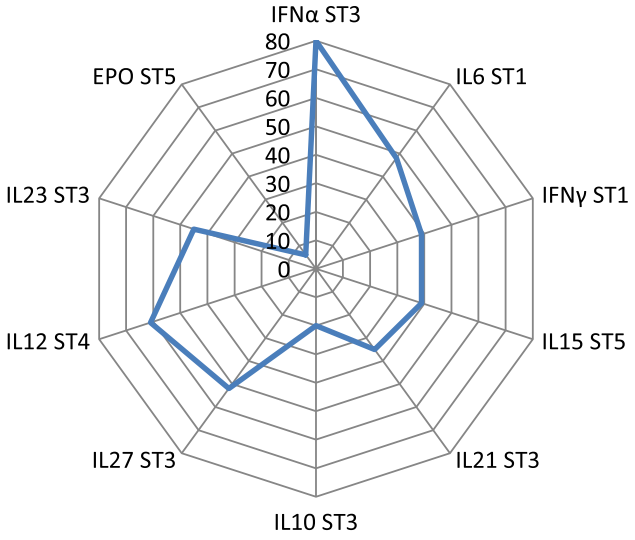

Fig. 10. Radial plot of cytokine inhibition IC_{XX} relative to the IFNα IC_{80} for compound **19**, derived from potency in human whole blood assays and predicted average daily human plasma drug concentration.

Table 5
Human whole blood IC50 values for each cytokine and associated JAK signaling pair.

Cytokine	JAK kinase pair	STAT	HWB $IC_{50(u)}$ (nM)[a]
IFNα	JAK1/TYK2	STAT3	42
IL6	JAK1/Jak2	STAT1	183
IFN γ	JAK1/JAK2	STAT1	265
IL15	JAK1/JAK3	STAT5	265
IL21	JAK1/JAK3	STAT3	319
IL10	JAK1/TYK2	STAT3	659
IL27	JAK1/JAK2	STAT3	155
IL12	TYK2/JAK2	STAT4	108
IL23	TYK2/JAK2	STAT3	207
EPO	JAK2/JAK2	STAT5	2519

[a] Compounds were assayed at least twice, and the IC_{50} reported as the geometric mean.

1.1. Synthesis

We have previously described the synthesis of compounds **7** − **9**[a] and we will focus on the synthetic replacement of the functionalized diamine core of **8** with 3-azabicyclo[3.1.0]hexan-1-amine as shown in Scheme 1. Commercially available 2,4-dichloro-5-fluoropyrimidine was substituted *via* direct displacement of the 4-chloride with ethanethiol as the nucleophile. At room temperature, the reaction was highly selective for displacement at the pyrimidyl 4-chloride driven in part by the

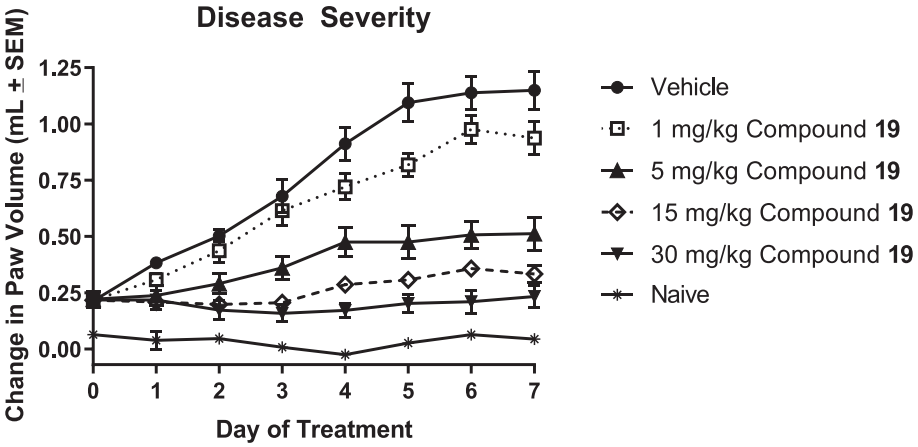

Fig. 11. Effect of compound **19** in the rat adjuvant-induced arthritis model following oral dosing of 1–30 mg/kg.

pyrimidine 5-fluoro presumably due to increased electrophilicity at this position. The pyrazole-2-amino pyrimidine intermediate **22** was constructed *via* S_NAr under acidic conditions using **21** and 2-(4-amino-1*H*-pyrazol-1-yl)ethan-1-ol. Oxidation to the sulfone **23** followed by displacement with commercially sourced *t*-butyl (3-azabicyclo[3.1.0]hexan-1-yl)carbamate afforded a mixture of compounds **24** and **25**. Compound **24** and **25** were separated by chiral supercritical fluid - chromatography (SFC). The protecting groups were removed under standard acidic conditions followed by amide coupling with either cyclopropane carboxylic acid, or *trans*-cyano cyclopropane carboxylic acid using HATU providing acetylated analogs **10, 11** and **28**. Chiral SFC separation of compound **28** provided analogs **13** and **14**.

The synthesis of the 6-methyl-3-azabicyclo[3.1.0]hexan-1-amine cores are described in Scheme 2. We utilized an intramolecular cyclopropanation reaction of a nitrile and di-substituted alkene described by Cha and coworkers to achieve the 6-substituted 3-azabicyclo[3.1.0]hexan-1-amine core.[23] The key intermediate **29** was made through alkylation of benzyl amine with 2-bromoacetonitrile followed by a second alkylation using 1-bromobut-2-yne. Subsequent hydrogenation with Lindlar catalyst set the required (*Z*) configuration of the olefin **31**. The stereospecific intramolecular cyclopropanation reaction was achieved using $Ti(OiPr)_4$ and cyclohexyl Grignard reagent to provide the *trans*-racemic mixture **32**. This mixture was purified by preparative SFC to afford intermediates **33** and **34**. Manipulation of the protecting groups would prove useful in our modular approach to final target synthesis. Therefore, Boc protection of **33** using standard conditions followed by hydrogenation (50 psi) with Pearlman's catalyst afforded key building block **36**.

Assembly of the final compounds was performed in a modular fashion by routes described in Scheme 3 and Scheme 4. The route illustrated in Scheme 3 incorporates the acetylated portion of the molecule first followed by construction of the pyrazole-2-amino

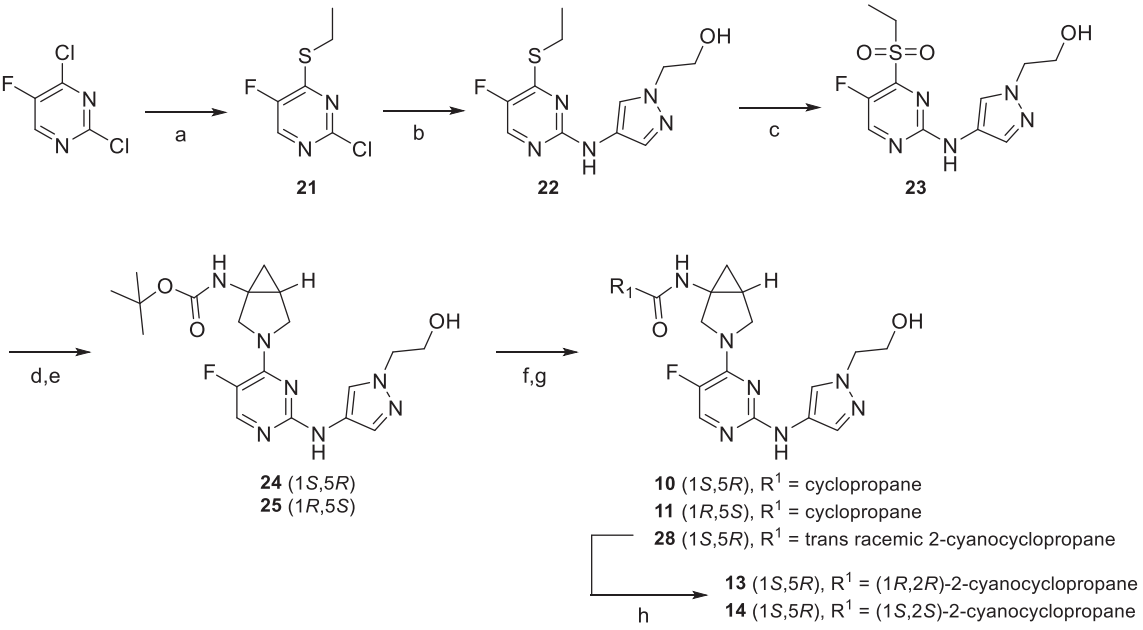

Scheme 1. *Reagents and conditions*. (a) ethanethiol, potassium *t*-butoxide, DME, 0 °C – RT, 36 h (76%); (b) 2-(4-amino-1*H*-pyrazol-1-yl)ethan-1-ol hydrochloride, 12 M HCl, *n*-butanol, 130 °C, 16 h (56%); (c) oxone, THF, 15 °C, 16 h (38%); (d) *t*-butyl (3-azabicyclo[3.1.0]hexan-1-yl)carbamate, TEA, MeCN, RT – 90 °C, 16 h (48%); (e) chiral SFC (45%); (f) **24** or **25**, con. HCl, dioxane, MeOH, RT, 3 h (100%); (g) **26** or **27**, R^1 carboxylic acid, HATU, TEA, DMF, RT, 3 h (49–63%); (h) chiral SFC (24–32%).

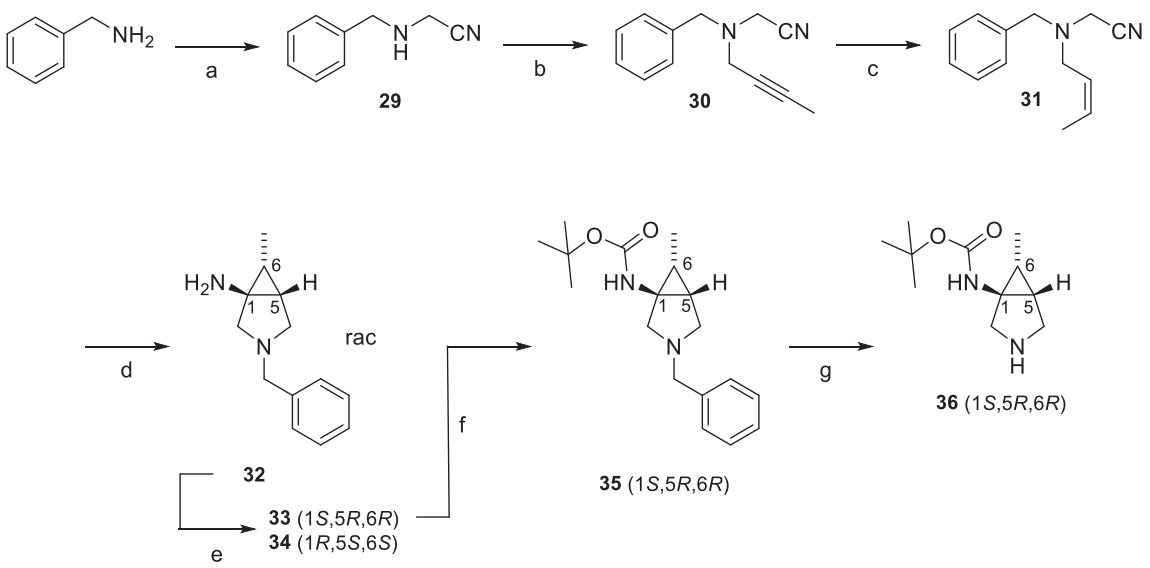

Scheme 2. *Reagents and conditions*. (a) 2-bromoacetonitrile, DIPEA, ACN, RT, 3 h (94%); (b) 1-bromobut-2-yne, K_2CO_3, ACN, 40 °C, 18 h (77%); (c) Lindlar catalyst, H_2, MeOH, 30 °C, 24 h; (d) $Ti(OiPr)_4$, cyclohexylmagnesium chloride (2 M in ether), THF, 20–30 °C, 3.5 h (36%); (e) chiral SFC; (f) ditertbutyldicarbonate, TEA, DCM, RT, 18 h (91%); (g) $Pd(OH)_2$, H_2 (50 psi), MeOH, RT, 48 h (100%).

pyrimidine moiety. Beginning with the *trans*-racemic intermediates **32**, the amides **37** were made through standard coupling conditions or in this case using the acid chloride. Benzyl deprotection using hydrogenation conditions previously described afforded **38** and subsequent S_NAr with 2,4-dichloro-5-fluoropyrimidine provided **39**. Purification under chiral SFC conditions provided the single enantiomers (**40** and **41**) and the hinge binding moiety of **40** was completed using acidic S_NAr conditions to provide compound **12**.

Scheme 4 describes the construction of the hinge binding motif followed by the late stage variation of the amide moiety. **36** underwent

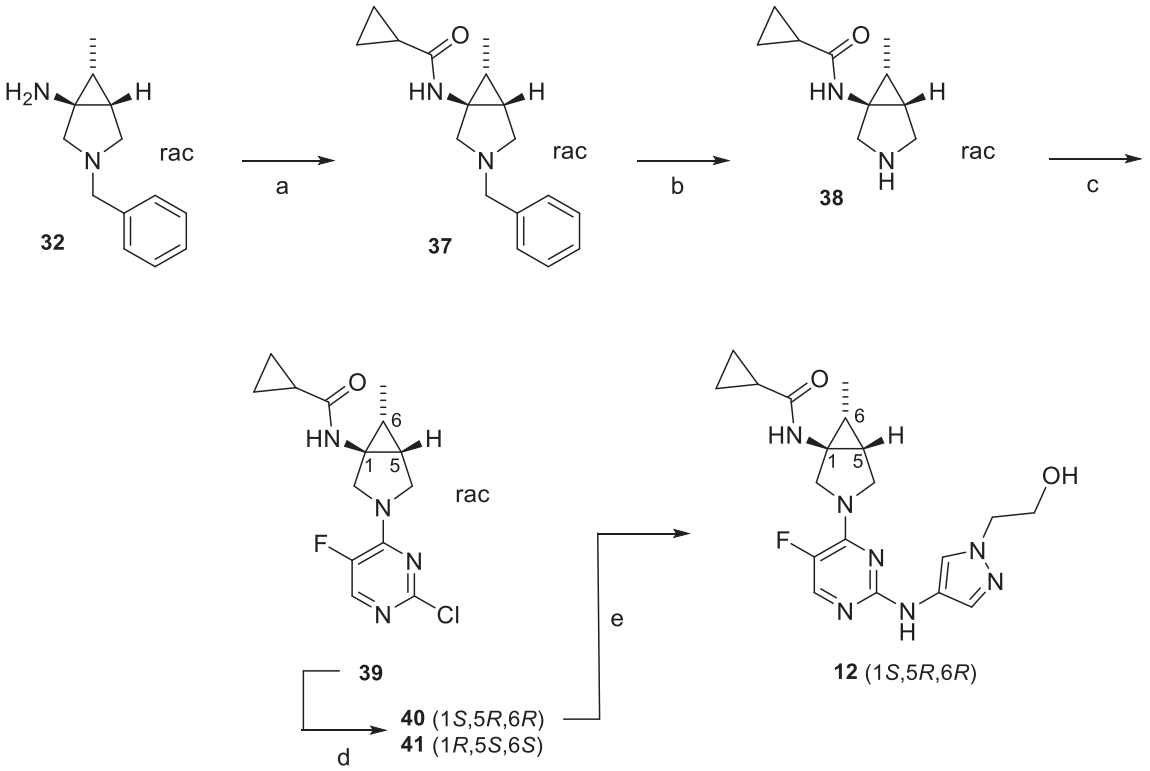

Scheme 3. *Reagents and conditions*. (a) cyclopropanecarbonyl chloride, TEA, CH_2Cl_2, RT, 1 h (77%); (b) $Pd(OH)_2$, H_2 (50 psi), MeOH, RT, 16 h; (c) 2,4-dichloro-5-fluoropyrimidine, TEA, MeOH, RT, 1 h (70% over 2 steps); (d) chiral SFC (36%); (e) 2-(4-amino-1*H*-pyrazol-1-yl)ethan-1-ol hydrochloride, IPA, 140 °C *mw*, 1 h (38%).

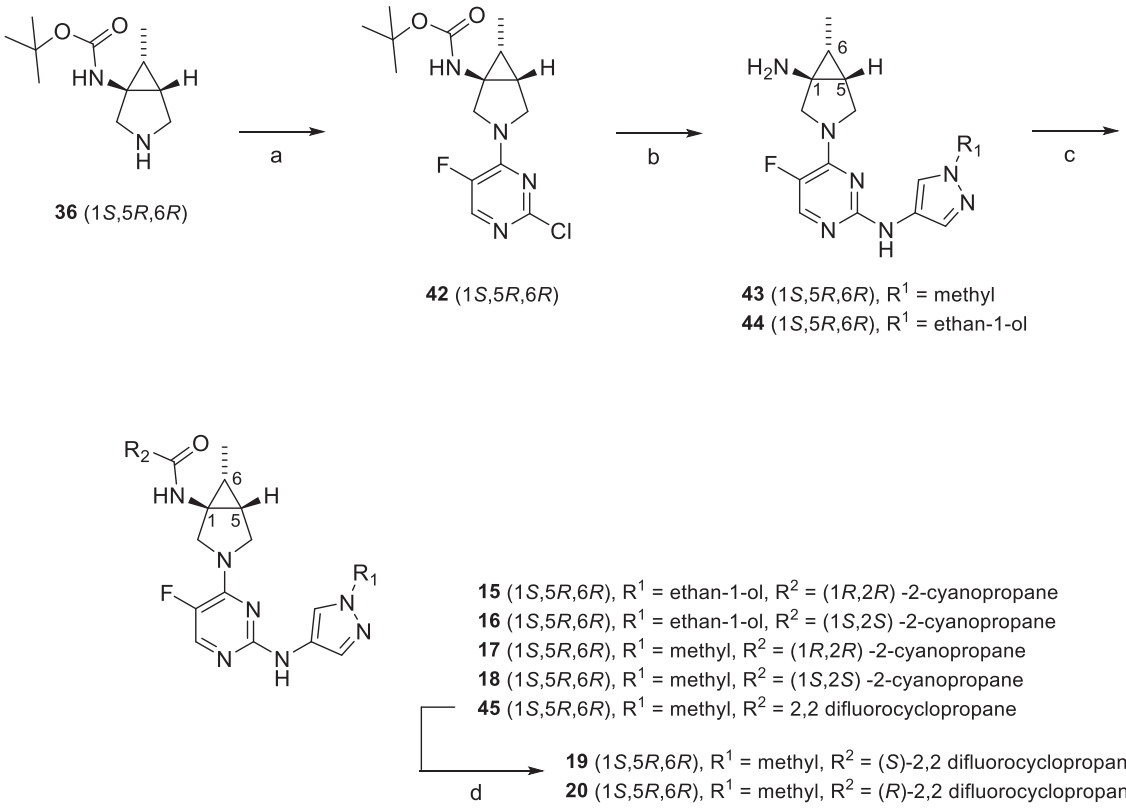

Scheme 4. *Reagents and conditions*. (a) 2,4-dichloro-5-fluoropyrimidine, TEA, MeOH, RT, 18 h (69%); (b) 1-methyl-1*H*-pyrazol-4ylamine hydrochloride or 2-(4-amino-1H-pyrazol-1-yl)ethan-1-ol hydrochloride (0.239 g, 1.46 mmol), IPA, 140 °C *mw*, 1 h (86–94%); (c) R^2 carboxylic acid, HATU, TEA or DIPEA, DCM or DMA, RT, 1.5–18 h (75–93%); (h) chiral SFC.

selective S_NAr with 2,4-dichloro-5-fluoropyrimidine at the 4-position to provide the substituted product **42** in 69% yield. The substituted pyrazole-2-amino pyrimidine moiety was made through a second S_NAr reaction under acidic conditions. The reaction conditions also resulted in the loss of the Boc group on the [3.1.0] azabicycle to provide **43** or **44** in excellent yields. Amide formation using **43** or **44** and various carboxylic acids[c] under standard HATU conditions provided **15–18** and **45**. Chiral SFC purification of **45**, provided **19** and **20** as single enantiomers.

2. Notes

2.1. Disclosures

The authors were employees of Pfizer Inc. during this work and declare no competing interest.

All activities involving laboratory animals were carried out in accordance with federal, state, local and institutional guidelines governing the use of laboratory animals in research and were reviewed and approved by Pfizer (or other) Institutional Animal Care and Use Committee. Pfizer animal care facilities that supported this work are fully accredited by AAALAC International.

3. PDB ID code

The atomic coordinates for the X-ray structure of JAK1 with compound **10** can be accessed from the RCSB Protein Data Bank (www.rcsb.org) using PDB code 6W8L. Atomic coordinates for the TYK2 X-ray structures with compounds **10**, **13**, **14** and **19** can be accessed using PDB codes 6NVY, 6VNS, 6VNV and 6VNX respectively. Authors will release the atomic coordinates upon article publication.

Declaration of Competing Interest

The authors declare that they have no known competing financial interests or personal relationships that could have appeared to influence the work reported in this paper.

Acknowledgements

Funding for this work was provided by Pfizer, Inc.

The authors would like to thank David Hepworth for helpful comments during preparation of the manuscript. The authors would also like to acknowledge the contributions of Matthew Griffor and John Knafels (Pfizer) for provision of TYK2 protein reagents and crystallization expertise.

This research used resources at the Industrial Macromolecular Crystallography Association Collaborative Access Team (IMCA-CAT) beamline 17-ID, supported by the companies of the Industrial Macromolecular Crystallography Association through a contract with Hauptman-Woodward Medical Research Institute. This research used resources of the Advanced Photon Source, a U.S. Department of Energy (DOE) Office of Science User Facility operated for the DOE Office of Science by Argonne National Laboratory under Contract No. DE-AC02-06CH11357.

Appendix A. Supplementary material

Supplementary data to this article can be found online at https://doi.org/10.1016/j.bmc.2020.11l5481.

References

1. O'Sullivan LA, Liongue C, Lewis RS, Stephenson SE, Ward AC. Cytokine receptor

ARTICLE IN PRESS

signaling through the Jak-Stat-Socs pathway in disease. *Mol Immunol.* 2007;44:2497–2506.
2. Virtanen AT, Haikarainen T, Raivola J, Silvennoinen O. Selective JAKinibs: Prospects in Inflammatory and Autoimmune Diseases. *BioDrugs: Clin Immunotherapeutics, Biopharmaceut Gene Therapy.* 2019;33:15–32.
3. Clark JD, Flanagan ME, Telliez JB. Discovery and development of Janus kinase (JAK) inhibitors for inflammatory diseases. *J Med Chem.* 2014;57:5023–5038.
4. Fridman JS, Scherle PA, Collins R, et al. Selective inhibition of JAK1 and JAK2 is efficacious in rodent models of arthritis: preclinical characterization of INCB028050. *J Immunol (Baltimore, Md: 1950).* 2010;184:5298–5307.
5. Quintas-Cardama A, Vaddi K, Liu P, et al. Preclinical characterization of the selective JAK1/2 inhibitor INCB018424: therapeutic implications for the treatment of myeloproliferative neoplasms. *Blood.* 2010;115:3109–3117.
6. Parmentier JM, Voss J, Graff C, et al. In vitro and in vivo characterization of the JAK1 selectivity of upadacitinib (ABT-494). *BMC Rheumatol.* 2018;2:23.
7. Fensome A, Ambler CM, Arnold E, et al. Dual Inhibition of TYK2 and JAK1 for the Treatment of Autoimmune Diseases: Discovery of ((S)-2,2-Difluorocyclopropyl)((1 R, 5 S)-3-(2-((1-methyl-1 H-pyrazol-4-yl)amino)pyrimidin-4-yl)-3,8-diazabicyclo[3.2.1] octan-8-yl)methanone (PF-06700841). J Med Chem 2018;61:8597–612.
8. Banfield C, Scaramozza M, Zhang W, et al. The Safety, Tolerability, Pharmacokinetics, and Pharmacodynamics of a TYK2/JAK1 Inhibitor (PF-06700841) in Healthy Subjects and Patients With Plaque Psoriasis. *J Clin Pharmacol.* 2017.
9. Weinstein DM, Ryan M. Advances in the discovery and development of selective tyrosine kinase 2 (TYK2) inhibitors. *Med Chem Rev.* 2018;53:177–200.
10. Wrobleski ST, Moslin R, Lin S, et al. Highly Selective Inhibition of Tyrosine Kinase 2 (TYK2) for the Treatment of Autoimmune Diseases: Discovery of the Allosteric Inhibitor BMS-986165. *J Med Chem.* 2019;62:8973–8995.
11. Warren J. Leonard, J.-X. L., John J. O'Shea. The γc Family of Cytokines: Basic Biology to Therapeutic Ramifications. Immunity 2019;50:832–50.
12. Frieder J, Kivelevitch D, Haugh I, Watson I, Menter A. Anti-IL-23 and Anti-IL-17 Biologic Agents for the Treatment of Immune-Mediated Inflammatory Conditions. *Clin Pharmacol Ther.* 2018;103:88–101.
13. Dendrou CA, Cortes A, Shipman L, et al. Resolving TYK2 locus genotype-to-phenotype differences in autoimmunity. *Sci Transl Med.* 2016;8 363ra149.
14. Thorarensen A, Banker ME, Fensome A, et al. ATP-mediated kinome selectivity: the missing link in understanding the contribution of individual JAK Kinase isoforms to cellular signaling. *ACS Chem Biol.* 2014;9:1552–1558.
15. Di L, Whitney-Pickett C, Umland JP, et al. Development of a new permeability assay using low-efflux MDCKII cells. *J Pharm Sci.* 2011;100:4974–4985.
16. Zhu, H. Water's Role in Compound Design for Drug Discovery. CCG UGM and Conference, Montreal, Canada.
17. Varma MV, Steyn SJ, Allerton C, El-Kattan AF. Predicting Clearance Mechanism in Drug Discovery: Extended Clearance Classification System (ECCS). *Pharm Res.* 2015;32:3785–3802.
18. Hosea NA, Collard WT, Cole S, et al. Prediction of human pharmacokinetics from preclinical information: comparative accuracy of quantitative prediction approaches. *J Clin Pharmacol.* 2009;49:513–533.
19. Obach RS. Predicting clearance in humans from in vitro data. *Curr Top Med Chem.* 2011;11:334–339.
20. Dowty ME, Jesson MI, Ghosh S, et al. Preclinical to clinical translation of tofacitinib, a Janus kinase inhibitor, in rheumatoid arthritis. *J Pharmacol Exp Ther.* 2014;348:165–173.
21. Dowty MEL, Lin TH, Wang L, et al. An Updated Analysis of Invitro Cytokine Inhibition Profiles of a Number of Janus Kinase Inhibitors at Clinically Maningful Concentrations. *United Eur Gastroenterol J.* 2017;5.
22. Hegen M, Keith Jr JC, Collins M, et al. Utility of animal models for identification of potential therapeutics for rheumatoid arthritis. *Ann Rheumatic Dis.* 2008;67:1505–1515.
23. Astashko D, Lee HG, Bobrov DN, Cha JK. Stereochemistry of the Kulinkovich Cyclopropanation of Nitriles. *J Organic Chem.* 2009;74:5528–5532.